

# A predictive model for the adjustment of violin bows

Frédéric Ablitzer, Jean-Pierre Dalmont

Laboratoire d'Acoustique de l'Université du Maine (UMR CNRS 6613), Le Mans, France

Nicolas Dauchez

Laboratoire d'Ingénierie des Systèmes Mécaniques et des Matériaux, Supméca, Saint-Ouen, France

## Summary

The quality of a violin bow is generally thought to be essentially determined by the wood used to make the stick. However, skilled bow makers are able to ameliorate the playing properties of a bow by finely adjusting its tapering and camber. This study aims at a better understanding of the link between the adjustment and the mechanical behavior of a bow. A finite element model of a bow is developed. The stick as well as the hair are modeled with beam elements. A co-rotational formulation is adopted to allow for geometric nonlinearity. The model is used to analyze the static behavior of a bow subjected to modifications of camber. One result is that increasing camber favors a high hair tension, which also diminishes the lateral bending stiffness of the stick.

PACS no. 43.75.De

## 1. Introduction

As an interface between the player's arm and the string, the bow is an all-important element in violin playing. In spite of its apparent simplicity, it is a very elaborate mechanical device, which requires high expertise from bow makers to meet the demand of professional players.

The primary fonction of a bow (Fig. 1) is to maintain a hair ribbon under tension. This gives little latitude in the choice of the wood [1], since the stick must remain slender in spite of the high tension it has to withstand. Moreover, the bow as we know it today has a very standard geometry, which could lead one to believe that the quality of a bow only hangs on the wood used to make it. However, by doing subtle adjustments on the geometry of the stick, experienced bow makers have the ability to draw the best from different wood blanks with various mechanical properties, or even to adapt the playing qualities of a bow to the needs of a specific player. Actually, bow makers play with three main parameters when making a stick:

- wood (density, elasticity, and maybe damping);
- tapering, which denotes the gradually decreasing thickness along the stick;
- camber, which is the concave curvature of the stick.

For the choice of the wood, some bow makers combine their know-how with a scientific approach. They use specific equipment (such as a *Lucchimeter* [2], or *Lutherie Tools* [3]) to measure some of the wood properties. Regarding tapering and camber, however, a specific device aimed at assisting bow makers does not exist at present. The mastery of these conception parameters thus requires a high expertise from the bow maker. The aim of our study is to develop a tool based on a physical model, capable of predicting the mechanical behavior of a bow with regard to the adjustable design parameters.

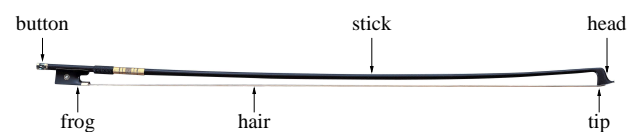


Figure 1. Modern violin bow.

In a previous study [4], an in-plane finite element model has been developed and used to investigate the static mechanical behavior of the bow resulting from different settings of camber and hair tension. Simulations have pointed out the nonlinear static behavior of the bow and shown that the compliance of the stick is significantly affected by camber. In this paper, the model is extended to take into account out-of-plane bending of the stick. In section 2, we present the finite element model and the generic geometry of

bow on which simulations are carried out. Numerical results are presented in section 3.

## 2. Model of the bow

### 2.1. General description

The model presented in this paper allows one to simulate, first, the tightening of the bow from its initial state without hair tension (Fig. 2.a) to its playing state (Fig. 2.b); then, the loading by a force on the hair, either vertical or inclined (Fig. 2.c). Throughout the simulation, the stick is clamped at the frog end and free at the other end. It should be noted that these boundary conditions are a simplified representation of actual playing conditions. However, they offer a convenient way to characterize the mechanical behavior as they can be easily reproduced experimentally.

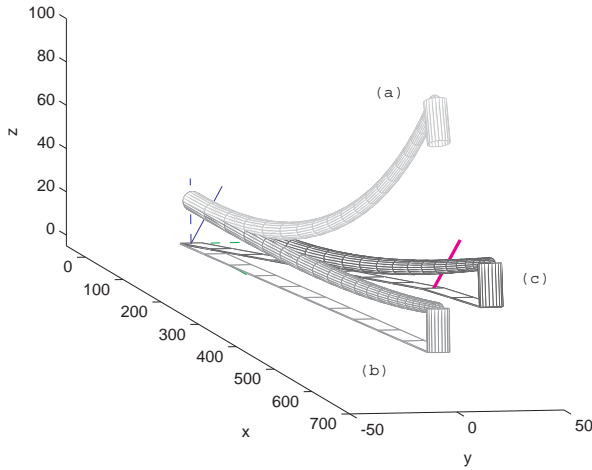


Figure 2. Model of the bow. (a) Initial shape of the stick, (b) tightened bow, (c) bow loaded by an inclined force.

The stick as well as the hair are modeled with Euler-Bernoulli beam elements. To take into account geometric nonlinearity, a large displacement formulation based on the co-rotational approach is adopted. The main steps of the formulation (after Crisfield [5]) are now presented.

### 2.2. Co-rotational formulation

The main idea of the co-rotational approach is to separate the total displacements of the structure into rigid-body motion and local deformation, as illustrated by Figure 3. The rigid-body motion can be arbitrarily large, while the local deformation is assumed to remain small. To each element is associated a local frame, materialized by base-vectors  $\mathbf{e}_1$ ,  $\mathbf{e}_2$  and  $\mathbf{e}_3$  in

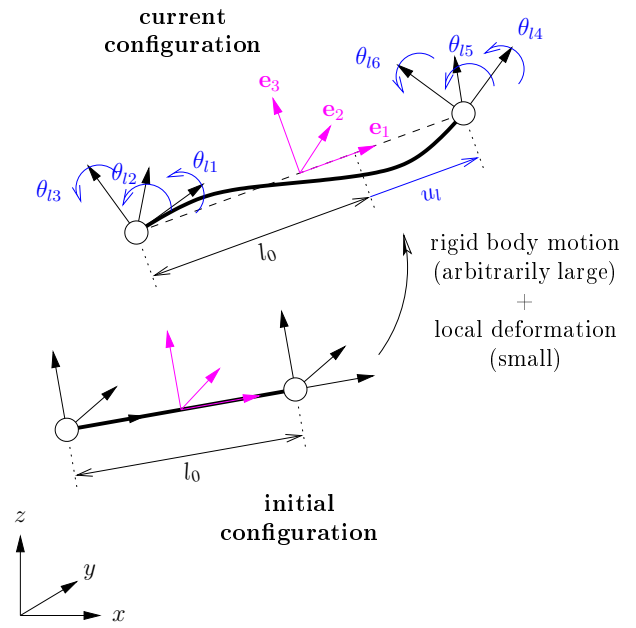


Figure 3. Illustration of the co-rotational approach.

Figure 3, which translates and rotates with the element.

In the local frame, the displacements caused by deformation are described by a set of “local” variables: axial elongation ( $u_l$ ), torsional angles ( $\theta_{l1}$  at node 1;  $\theta_{l4}$  at node 2), bending slopes ( $\theta_{l2}$ ,  $\theta_{l3}$  at node 1;  $\theta_{l5}$ ,  $\theta_{l6}$  at node 2). These local displacements, gathered in vector  $\mathbf{p}_l$ , are conjugate to local internal efforts  $\mathbf{q}_{il}$  (axial force, torsional moments, and bending moments, respectively). Since the local deformation is small, a linear relationship between local displacements and internal efforts can be written as:

$$\mathbf{K}_l \mathbf{p}_l = \mathbf{q}_{il} , \quad (1)$$

where  $\mathbf{K}_l$  is the local stiffness matrix ( $7 \times 7$ ), which remains the same during the analysis.

In any deformed configuration of the structure, the local displacements  $\mathbf{p}_l$  can be computed from the “global” displacements  $\mathbf{p}$ , which relate to the global frame and consist of 3 translations and 3 rotations per node. Moreover, it is possible to express a relationship between infinitesimal changes of local and global displacements, resp.  $\delta \mathbf{p}_l$  and  $\delta \mathbf{p}$ , as:

$$\delta \mathbf{p}_l = \mathbf{F} \delta \mathbf{p} , \quad (2)$$

where  $\mathbf{F}$  is the transformation matrix ( $7 \times 12$ ). Contrary to the local stiffness matrix,  $\mathbf{F}$  depends on displacements and has to be computed at each iteration. Knowing the transformation matrix, it is possible to relate the global internal efforts  $\mathbf{q}_i$  to the local internal efforts  $\mathbf{q}_{il}$  given by Eq. (1). For this, we express the fact that the internal virtual work has to be the same in the global and local frame, which yields:

$$\mathbf{q}_i = \mathbf{F}^T \mathbf{q}_{il} . \quad (3)$$

The last step in the formulation is to express the tangent stiffness matrix  $\mathbf{K}_t$ . The static equilibrium of the structure is expressed by:

$$\mathbf{g} = \mathbf{q}_i - \mathbf{q}_e = \mathbf{0}, \quad (4)$$

where  $\mathbf{g}$  is the vector of out-of-balance efforts and  $\mathbf{q}_e$  the vector of external efforts, which are assumed here to be independent of the displacements. Assuming that the structure at iteration ( $i$ ) is not in equilibrium and expanding  $\mathbf{g}$  in a first-order Taylor series about the current displacements  $\mathbf{p}^{(i)}$ , Eq. (4) becomes:

$$\mathbf{g}^{(i)} + \left. \frac{\partial \mathbf{g}}{\partial \mathbf{p}} \right|_{\mathbf{p}^{(i)}} \delta \mathbf{p}^{(i+1)} = \mathbf{0}, \quad (5)$$

where  $\delta \mathbf{p}^{(i+1)}$  is the vector of incremental displacements between the current and next iteration, i.e.  $\mathbf{p}^{(i+1)} = \mathbf{p}^{(i)} + \delta \mathbf{p}^{(i+1)}$ . The tangent stiffness matrix is then:

$$\begin{aligned} \mathbf{K}_t &= \frac{\partial \mathbf{g}}{\partial \mathbf{p}} = \mathbf{F}^T \frac{\partial \mathbf{q}_{il}}{\partial \mathbf{p}} + \frac{\partial \mathbf{F}^T}{\partial \mathbf{p}} \mathbf{q}_{il} \quad \text{after (3)} \\ &= \mathbf{F}^T \mathbf{K}_l \mathbf{F} + \frac{\partial \mathbf{F}^T}{\partial \mathbf{p}} \mathbf{q}_{il}. \end{aligned} \quad (6)$$

The first term in  $\mathbf{K}_t$  corresponds to natural elastic stiffness (dependent on material and cross-section properties), and the second to geometric stiffness, due to the stress field in the structure.

### 2.3. Generic geometry of the bow

The tapered profile is derived from a formula given by Vuillaume. This violin maker of the 19th century measured a great number of Tourte bows and found the diameter to decrease logarithmically along the stick [6]. The diameter  $d$  at abscissa  $x$  ( $0 \leq x \leq 650$  mm) is given by:

$$d(x) = d_0 \left( 1 + \varepsilon \ln \left( \frac{x_\infty - x}{x_\infty} \right) \right), \quad (7)$$

where  $d_0 = 8.77$  mm,  $x_\infty = 825$  mm and  $\varepsilon = 0.255$ .

The distribution of camber along the bow is here defined so that the stick becomes straight under a “maximal” tension, which is a criteria commonly recognized by bow makers [7]. In this configuration, the distance between hair and neutral axis of the stick is constant, assuming that the frog and the head have the same height  $h$ . Thus, the bending moment resulting from maximal hair tension  $T_0^{\max}$  has a constant value  $\mathcal{M}_0^{\max} = h T_0^{\max}$  along the stick. The initial curvature of the stick can be determined by calculating the deformed shape of the initially straight stick subject to moment  $\mathcal{M}_0^{\max}$  at its free end. The value of  $T_0^{\max}$  determines the amount of camber, which can be also characterized by the minimal hair-stick distance without tension, denoted by  $\kappa$  in the following.

## 3. Results from simulations

In this section, we examine the compliance of the bow and its behavior for different loading cases (vertical/inclined force, low/high amplitude). For this purpose, simulations are carried out on the standard bow with “full camber” ( $\kappa = 0$  mm), tightened up to an hair-stick distance of 10 mm. Then, we evaluate the influence of two parameters on compliance: hair tension and camber. In all simulations, the Young’s modulus of the stick is  $E_s = 25$  GPa. The cross section ( $0.39$  mm  $\times$   $1$  mm) and Young’s modulus ( $E_h = 5$  GPa) of the hair give an equivalent longitudinal compliance of  $30$  N/mm for a  $65$  cm ribbon.

### 3.1. Compliance of the bow

Since the bow is often slightly tilted towards the fingerboard in playing (generally up to  $30^\circ$ ), the stick bends in both lateral and vertical directions. To take this into account in the simulations, the force applied to the hair is inclined by angle  $\psi$  relatively to the bow reference frame (Fig. 4).

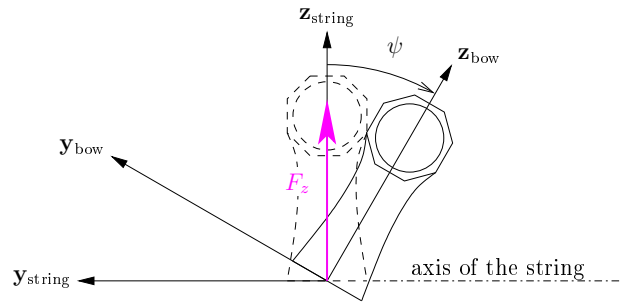


Figure 4. Rear view of the bow in its reference frame, the x-axis of which is defined by the line joining the front end of the frog and the tip.

Figure 5 shows the simulated deflection at the tip caused by a force  $F_z$ , for two values of tilt angle,  $\psi = 0^\circ$  (“vertical”), and  $\psi = 30^\circ$  (“inclined”). In both cases, the evolution of deflection with force is nonlinear. The compliance, which we define as the slope of the force-deflection curve, increases with force. Moreover, the compliance is higher when the force is inclined. This has a simple interpretation: when out-of-plane bending of the stick occurs, the hair tension exerts an additional bending moment along the stick. This moment acts together with that caused by the force, which makes the deflection higher.

In the following, we examine the compliance of the bow at  $F_z = 0$  N and at  $F_z = 1.5$  N, in an attempt to characterize the behavior of the bow at both low and high forces (e.g. when playing *pianissimo* and *fortissimo*, respectively). Although bow forces higher than  $1.5$  N are not unrealistic in playing, this value can be

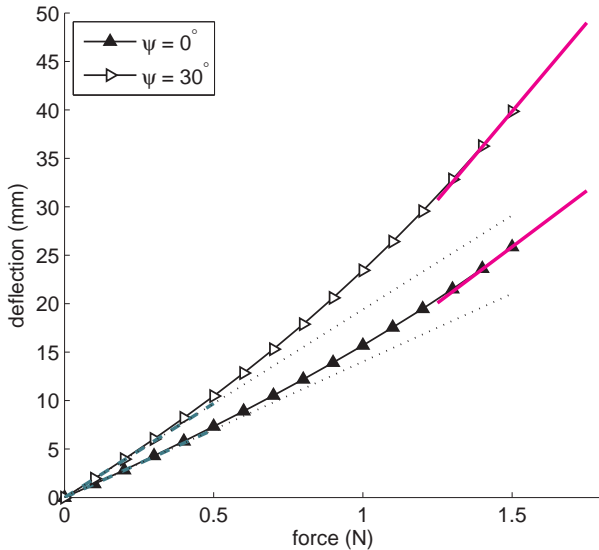


Figure 5. Deflection vs amplitude of vertical ( $\psi = 0^\circ$ ) and inclined ( $\psi = 30^\circ$ ) force  $F_z$  at the tip. The deviation from a linear evolution (dotted lines) indicates a nonlinear compliance, defined as the slope of the force-deflection curve (represented here at  $F_z = 0$  N and  $F_z = 1.5$  N).

considered as an upper limit when playing near the tip.

Figure 6 shows the compliance along the bow at low and high forces. For all the simulated load cases, the compliance continuously increases along the bow, reaching its maximal value at the tip. Regarding the vertical compliance, two kinds of nonlinearity are observed. In the first two thirds of the bow length, increasing the force diminishes the compliance. This is due to a rise in hair tension that makes the hair stiffer. In the last third, conversely, the compliance increases with force. The inclined compliance also exhibits this kind of nonlinearity, but on a longer portion of the bow (second half). At low forces as well as at high forces, tilting the bow offers a higher compliance.

Keeping in mind that the stick on its own behaves linearly when loaded by a similar force along its length and has the same bending stiffness in lateral and vertical directions (see Fig. 6, “stick only”), the range in compliance offered by the assembled, tightened bow is remarkable. In the simulation presented here, the compliance at the tip varies between 14.0 mm/N and 36.5 mm/N (respectively,  $-18\%$  and  $+112\%$  with regard to the compliance of the stick only). In the following, we focus on the compliance at the tip, in order to show how hair tension and camber affect the behavior of the stick.

### 3.2. Influence of hair tension

Starting from the assembled bow at zero tension, the hair tension  $T_0$  was increased up to maximum tension  $T_0^{\max}$ , at which the stick is straight. At each tight-

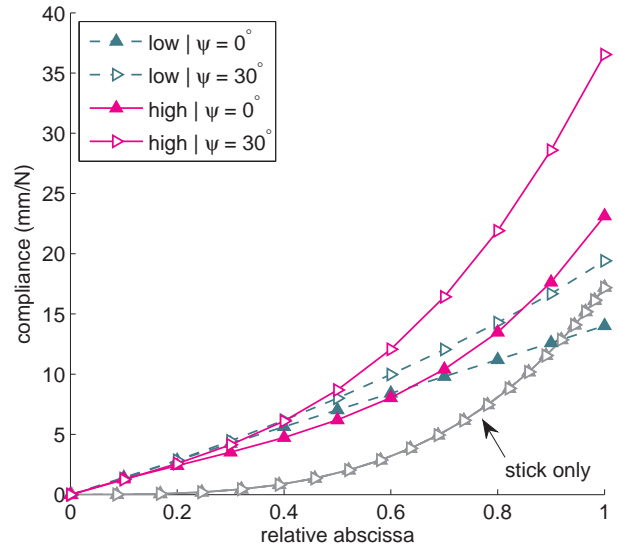


Figure 6. Vertical ( $\psi = 0^\circ$ ) and inclined ( $\psi = 30^\circ$ ) compliance along the bow, at low forces ( $F_z = 0$  N) and high forces ( $F_z = 1.5$  N). The compliance along the stick without the hair, obtained with the same four load cases, is plotted too.

ening step, the compliance at the tip for a vertical and inclined force ( $\psi = 0^\circ$  and  $30^\circ$ , respectively) was computed. Figure 7 shows the numerical results.

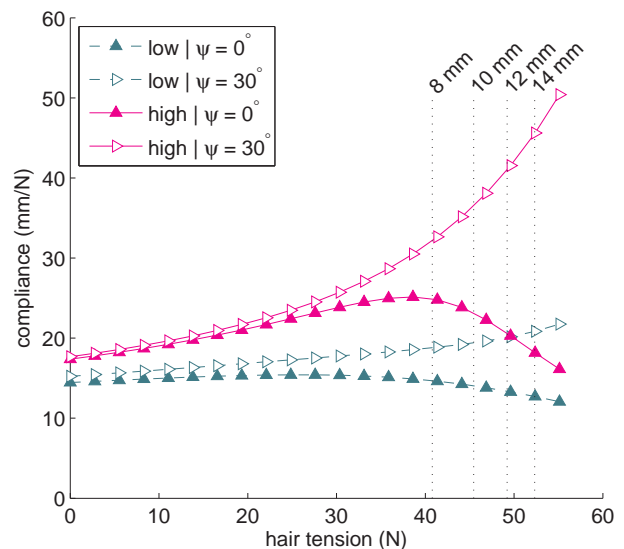


Figure 7. Vertical ( $\psi = 0^\circ$ ) and inclined ( $\psi = 30^\circ$ ) compliance at the tip vs hair tension, at low forces ( $F_z = 0$  N) and high forces ( $F_z = 1.5$  N). Dotted lines indicate values of hair tension corresponding to four values of hair-stick distance (from 8 mm to 14 mm).

It clearly appears that the gap between vertical and inclined compliance increases with the hair tension. Regarding vertical compliance at high forces, it should

be noted that the range between  $T_0 = 0$  N and  $T_0 = 40$  N is of little relevance, since a vertical force of 1.5 N makes the stick go through the hair. Of most interest is the range marked by dotted lines, for which the hair-stick distance is comprised between 8 mm and 14 mm, thus corresponding to plausible settings for playing the bow. Moreover, it is in this region that the gap between vertical and inclined compliance varies the most with hair tension, especially at high forces.

### 3.3. Influence of camber

The same load cases as in section 3.2 were simulated for two amounts of camber, corresponding to two values of minimal hair-stick distance without tension:  $\kappa = 4$  mm and  $\kappa = 0$  mm. Figure 8 shows the compliance at the tip plotted against hair tension, in the range around plausible values of hair-stick distance for playing. It should be noted that the two variants of the bow when tightened up to a same value of hair-stick distance, are indistinguishable from one another. This is because only the amount of camber was changed, not its distribution along the stick.

First, increasing the amount of camber allows to increase the playing hair tension. Considering a playing hair-stick distance of 10 mm, for example, increasing camber from  $\kappa = 4$  mm to  $\kappa = 0$  mm gives 66% more hair tension. Moreover, the range in compliance at a given hair-stick distance significantly increases with camber, as well as the ratio between inclined and vertical compliance. It also appears that the range in compliance offered by the bow is more sensitive to the setting of hair tension when camber increases. It would be tempting to deduce from these observations that the same bow offers more potential to the player when it is much cambered than less. Playing tests are needed to better apprehend the consequences on playing.

## 4. Conclusion

A finite element model of violin bow has been developed and used to investigate the static behavior of the tightened bow. In particular, the influence of tilting the bow on compliance has been examined.

Simulations have shown that the compliance, which also depends on force, is higher when the bow is tilted. An important result is that the compliance of the assembled, tightened bow considerably varies with regard to that of the stick only. The range in compliance offered by the bow is affected by parameters adjustable by the player (hair tension) and by the bow maker (camber).

Playing tests of parametrized bows will be presented. The aim is to evaluate how the player perceives changes in hair tension and camber. If significant trends emerge from this study, the model could

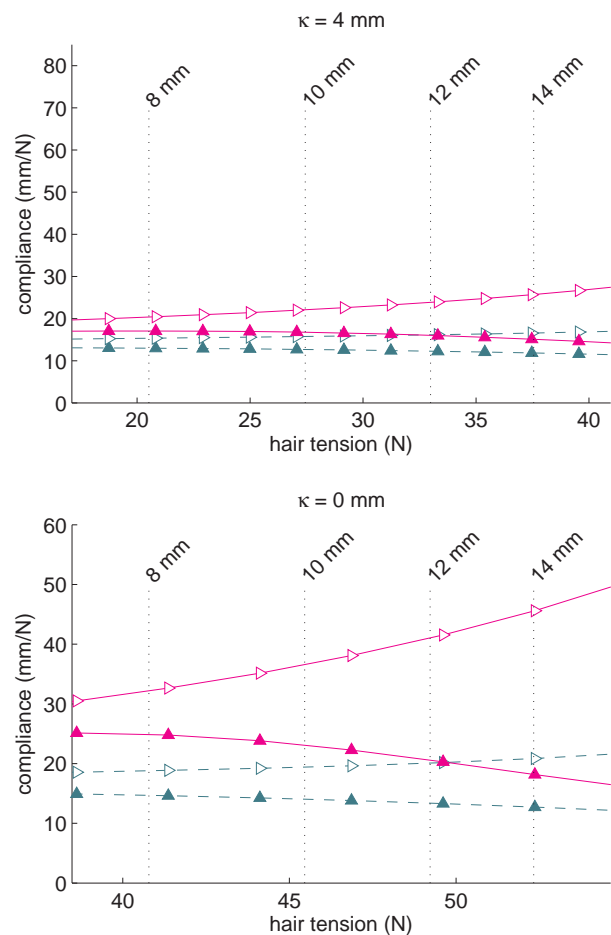


Figure 8. Vertical and inclined compliance at low and high forces (see legend of Fig. 7), for two settings of camber, characterized by minimal hair-stick distance without hair tension  $\kappa$ .

be useful to assist bow makers in adjusting the geometry of a stick so as to reach a given behavior on the assembled, tightened bow.

### Acknowledgement

The study presented in this paper was partially supported by the French National Research Agency (ANR) within the PAFI project.

### References

- [1] U. Wegst, S. Oberhoff, M. Weller, and M. Ashby. Materials for violin bows. *International Journal of Materials Research*, 98:1230–1237, 2007.
- [2] G. Lucchi & Sons, <http://www.lucchiremona.com/>. last viewed 17 March 2011.
- [3] F. Gautier, V. Doutaut, and J.-M. Fouilleul. *Lutherie tools : projet collaboratif entre ateliers de lutherie et laboratoires. Musique & Technique*, 4:21–28, 2009.
- [4] F. Ablitzer, J.-P. Dalmont, and N. Dauchez. Static model of a violin bow: influence of camber and hair tension on mechanical behavior. Accepted for publication in the *J. Acoust. Soc. Am.* (2011).

- [5] M. A. Crisfield. *Non-linear finite element analysis of solids and structures*, volume 2. Wiley, Chichester, 1997.
- [6] F.-J. Fétis and J. Bishop. *Notice of Anthony Stradivari, the celebrated violin-maker, known by the name of Stradivarius*, chapter Experimental determination of the form of Tourte's bows, pages 121–124. R. Cocks and co., London, 1864.
- [7] B. Rolland. The playing parts of the bow: focusing on the stick. *Journal of the Violin Society of America*, 19(1):201–217, 2002.